Power Electronic Systems
Laboratory

Proceedings of the XXIIth International Conference on Electrical Machines (ICEM'2016) , Lausanne, Switzerland, September 4-7, 2016

Rotor Losses in an Ultra-High Speed Spinning Ball Motor

M. Schuck,
D. Steinert,
J. W. Kolar

Eidgenössische Technische Hochschule Zürich
Swiss Federal Institute of Technology Zurich

Rotor Losses in an Ultra-High Speed Spinning Ball Motor

Marcel Schuck, *Student Member, IEEE*, Daniel Steinert, *Member, IEEE* and Johann W. Kolar, *Fellow, IEEE*

***Abstract*—The ongoing miniaturization trend of electric machines demands for higher rotational speeds to provide a required power level at decreased size. The goal of this project is to push the limits of miniaturization by researching new concepts for bearingless machines with ultra-high rotational speeds exceeding 25 million rotations per minute (Mrpm). The employed sub-millimeter size spherical solid steel rotors are accelerated by the principle of a solid rotor induction machine. This study presents an analysis of the resulting eddy current losses and a thermal model of the rotor. The temperature of the rotor material is of interest, as it influences the achievable rotational speed at which failure of the rotor due to centrifugal loading occurs.**

***Index Terms*—asynchronous machine, magnetic bearing, rotor losses, spinning ball, ultra-high speed.**

I. Introduction

THE ongoing trend towards the miniaturization of electric machines demands for increased rotational speeds in order to achieve high power densities. Small size drive systems with rotational speeds of up to 1 Mrpm have been developed in the past [1]. The achievable rotational speeds are limited by the resulting losses, which are mostly generated by friction. The latter can effectively be reduced by using magnetic bearings. As air friction becomes significant at such high rotational speeds, additional measures are required to achieve even higher rotational speeds. By accelerating the rotor inside a vacuum, rotational speeds in excess of 20 Mrpm have been achieved in the past [2]. As the achievable rotational speed is ultimately limited by the tensile strength of the rotor material, sub-millimeter size solid steel spheres are used as rotors. At such scales, further limits are imposed by the controllability and precision of the employed magnetic bearing systems.

The goal of this project is to push the limits of miniaturization with an ultra-high speed motor reaching rotational speeds beyond 25 Mrpm. Ultimately, it is targeted at demonstrating the highest possible rotational speed with an electric motor. The conducted research helps to extend the limits of conventional machines and to overcome the challenges in regard to power density, mechanical stress and controllability of highly dynamic systems. Moreover, the applicability of highly precise magnetic bearings for levitation and stabilization of rotors in the sub-millimeter range is demonstrated.

The authors would like to thank the Else & Friedrich Hugel Fund for Mechatronics for supporting this work.

M. Schuck and J. W. Kolar are with the Power Electronic Systems Laboratory, Swiss Federal Institute of Technology (ETH) Zurich, 8005 Zurich, Switzerland (e-mail: schuck@lem.ee.ethz.ch).

D. Steinert is with Levitronix GmbH, 8005 Zurich, Switzerland

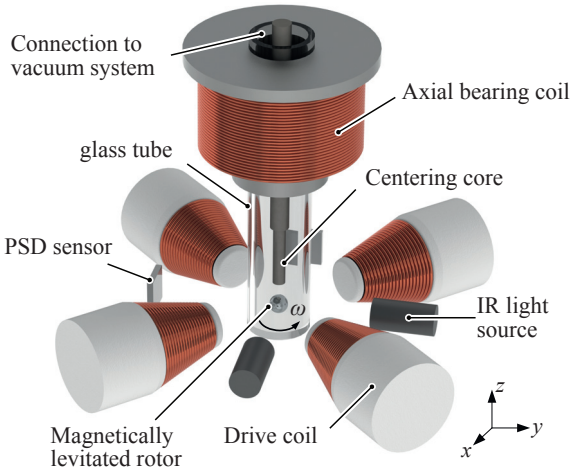

Fig. 1: Setup of the ultra-high speed motor.

The drive system for acceleration of the rotor is based on the principle of a solid rotor induction machine. Therefore, eddy currents are induced inside the rotor, which result in ohmic losses due to the finite conductivity of the rotor material. These losses may cause a significant increase of the rotor temperature, which in turn decreases its tensile strength [3], [4]. The resulting effects have been observed during acceleration experiments, where spheres which had been accelerated with a higher torque were prone to fail at comparably lower rotational speeds than spheres which had been accelerated more slowly. For very high torques, a deformation of the spherical rotor due to the high centrifugal forces and the softening of the rotor material, resulting in an ellipsoidal shape, could be observed.

This study presents a thermal model of the spherical rotor of the ultra-high speed motor based on complete analytical solutions of the underlying field problem. It provides the necessary solutions to determine the resulting rotor temperature for a given torque and magnetic flux density inside the motor. Conversely, the developed model also allows to optimize the drive parameters such that high acceleration torques are achieved with minimal rotor temperature, thus not negatively affecting the stability and tensile strength of the rotor material.

The remainder of this paper is organized as follows: Section II briefly describes the motor setup and in Section III complete analytic solutions for the eddy current distribution

978-1-5090-2538-1/16/$31.00 ©2016 IEEE

inside the rotor and the motor torque, based in the underlying field problem inside the motor, are outlined. These are used in Section IV to determine the ohmic rotor losses and to develop a thermal model of the rotor. Section V presents a thermal optimization which determines the optimal slip frequency of the motor at which the highest torque to loss ratio is attained. This optimal slip frequency is used to calculate absolute values of the rotor torque and temperature, which provide the aforementioned guidelines for choosing the motor parameters for a given admissible rotor temperature. Section VI concludes the paper.

II. Motor Setup

The developed ultra-high speed motor setup is shown in Fig. 1. The rotor is placed inside an evacuated glass tube to minimize air friction. Bearing friction is eliminated by using an axial magnetic bearing, which is constructed from a copper coil wound around a hollow ferromagnetic core to allow sufficient space for positioning of the vacuum tube through the core. A second, solid ferromagnetic cylinder is placed directly inside the vacuum tube to act as a centering core which concentrates the magnetic flux and is the center of attraction for the levitated rotor.

In addition to the axial bearing, four air coils are placed radially around the rotor to produce the fast rotational magnetic fields required for torque generation. Acceleration is achieved by the principle of a solid rotor induction machine, where eddy currents are induced inside the rotor, which are subject to tangential Lorentz forces.

As there is almost no air friction acting upon the rotor, radial oscillations due to disturbances are weakly damped, causing the magnetic suspension to become unstable. Therefore, the radially-placed coils are also used as actuators for a radial AMB, which increases the radial damping of the system.

For the magnetic suspension to operate properly, the axial and radial rotor position has to be measured and controlled continuously. In the developed setup, the rotor is illuminated by two orthogonally-placed infrared light sources resulting in a rotor shadow being drawn onto two two-dimensional position sensitive device (PSD) sensors, which are placed on the opposite side of the vacuum glass tube. The resulting position signals are fed into digital PID controllers, which regulate the rotor position by adjusting the currents in the axial and radial bearing coils.

With the developed setup, spherical rotors with diameters of 3 mm down to sub-millimeter sizes can be levitated and accelerated.

III. Solution of the Electromagnetic Field Problem

A torque $\vec{T}$ is exerted on the rotor of the solid rotor induction machine due to the interaction of the eddy current density $\vec{J}$ inside the rotor and the external magnetic drive field. To provide a complete analytical solution of the field problem as encountered in the motor in [5], the rotor has been assumed to be penetrated by a homogeneous magnetic flux density of magnitude B_0 which rotates with a frequency of ω_f. To provide an understanding of the underlying mathematical considerations, the relevant solutions are reproduced below and are used later on to obtain the motor torque and the rotor losses.

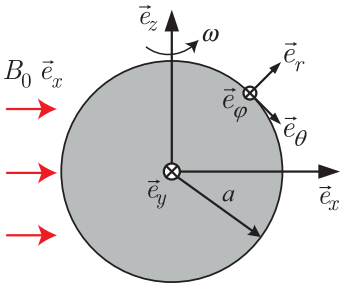

Fig. 2: Coordinate system as used for the calculations.

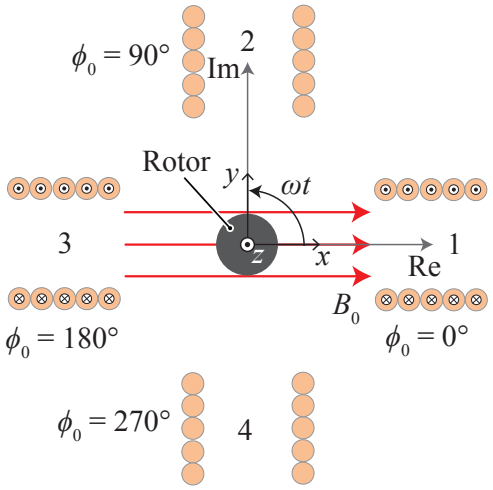

Fig. 3: Field of the drive coils for torque generation.

For all presented mathematical considerations, a coordinate system such as displayed in Fig. 2 with the rotor spinning around the z axis has been used. The generation of the drive field is illustrated in Fig. 3, where ω denotes the slip frequency, which is the difference of the mechanical rotational frequency of the rotor ω_mech and the rotational frequency of the magnetic flux density ω_f. To generate a rotating field, the currents in the coils denoted by 2, 3, and 4 have to be phase shifted by $90°$, $180°$, and $270°$ with respect to the current in coil 1, respectively. In the depicted instant, the field vector is pointing in the x direction, corresponding to the case where the currents in coils 1 and 3 reach their maximum, and minimum values, respectively and the currents in coils 2 and 4 are zero.

A. Current Density Inside the Rotor

A solution to the occurring field problem can be found by an ansatz based on the magnetic vector potential $\vec{A}$. The resulting current density distribution inside the rotor has been

obtained as (cf. [5])

$$\vec{J}(r,\varphi) = -\frac{1}{2}B_0\sigma\omega r\mathrm{Re}\left\{F(r)[-\cos\varphi - j\sin\varphi]\vec{e}_\theta e^{j\omega t}\right\}, \tag{1}$$

where $F(r)$ is the solution to the underlying differential equation as determined by the field problem and r and φ denote the positions inside the sphere in cylindrical coordinates. For the region inside the sphere

$$F(r) = [1 + D(c_{\mathrm{EC}}a)]\frac{f(c_{\mathrm{EC}}r)}{f(c_{\mathrm{EC}}a)} \tag{2}$$

holds, where a is the radius of the sphere. The remaining functions are given as

$$D(c_{\mathrm{EC}}a) = \frac{(2\mu_r+1)g(c_{\mathrm{EC}}a) - 1}{(\mu_r - 1)g(c_{\mathrm{EC}}a) + 1}, \tag{3}$$

$$g(c_{\mathrm{EC}}a) = f(c_{\mathrm{EC}}a)\frac{c_{\mathrm{EC}}a}{\sin(c_{\mathrm{EC}}a)}, \tag{4}$$

$$f(c_{\mathrm{EC}}r) = \frac{\sin(c_{\mathrm{EC}}r)}{(c_{\mathrm{EC}}r)^3} - \frac{\cos(c_{\mathrm{EC}}r)}{(c_{\mathrm{EC}}r)^2}, \tag{5}$$

and

$$c_{\mathrm{EC}} = \sqrt{-j\mu_0\mu_r\sigma\omega}, \tag{6}$$

with μ_r and σ denoting the relative permeability and the conductivity of the rotor material, respectively. It can be observed that the current density depends linearly on the magnitude of the external magnetic flux density B_0.

B. Motor Torque

To provide an analytical expression for the torque dependent on the rotor material, geometric parameters, and B_0, an approximation of the complete analytical results is presented in (44) of [5]. As this approximation yields inaccurate results for rotor materials with conductivities below $\sim 5\ \mathrm{MS/m}$ and rotor radii below $\sim 1\ \mathrm{mm}$, such as present in the ultra-high speed spinning ball motor, this approximation is not used in this work. Instead, a numerical calculation of the torque based on the complete analytical solution is performed.

The motor torque of the machine is calculated as the cross product of the magnetic dipole moment of the rotor and the external flux density as

$$\vec{T} = \vec{m} \times \vec{B}_0, \tag{7}$$

where

$$\vec{m} = \frac{2\pi}{\mu_0}a^3 B_0 \mathrm{Re}\left\{F(a)\begin{pmatrix}1\\ j\\ 0\end{pmatrix}\cdot\begin{pmatrix}\vec{e}_x\\ \vec{e}_y\\ \vec{e}_z\end{pmatrix}\right\} \tag{8}$$

contains the solution $F(a)$ as presented above, yielding

$$\vec{T} = -B_0 m_y \vec{e}_z. \tag{9}$$

Therefore, the torque depends quadratically on B_0.

To allow for fast acceleration of the rotor to ultra-high speeds, the angular acceleration of the rotor should be as high as possible. The latter is described by the relation

$$\dot{\omega}_{\mathrm{mech}} = \frac{T}{I}, \tag{10}$$

where I denotes the mass moment of inertia of the body, which is given as

$$I = \frac{8}{15}\rho\pi a^5 \tag{11}$$

for a solid sphere with constant mass density ρ rotating about an axis through its center of mass. Therefore, a high torque is desirable which can be accomplished for a given rotor size and material by

1) increasing the magnitude of the flux density B_0 at the rotor for high values,
2) choosing the slip frequency ω such that $\mathrm{Re}\{jF(a)\}$, as part of m_y, is maximized.

Option 1 is constrained by how well the magnetic flux density of the drive coils can be guided towards the rotor, the achievable drive current, and the resulting stator and rotor losses.

Option 2 is constrained by the fact that the frequency of the magnetic flux ω_f, and consequently the frequency of the drive currents, has to be higher than the desired rotational speed. If a constant torque is desired, ω_f has to be increased as ω_{mech} increases. If ω_f is kept constant, $\dot{\omega}_{\mathrm{mech}}$ will decrease as ω_{mech} increases.

As the tensile strength of the rotor material, which determines how well the rotor can withstand centrifugal forces at ultra-high rotational speeds, is decreased if its temperature is increased, an optimization of the motor torque requires the knowledge of the rotor losses and the resulting increase of the rotor temperature.

IV. Rotor Losses

The ohmic volume loss density due to eddy current losses inside the rotor can be calculated by using (1) as

$$p_{\mathrm{EC}} = \frac{1}{\sigma}\vec{J}^2. \tag{12}$$

Figure 4 shows the loss density inside the sphere in the xy-plane at $z = 0$ (cut through the equator) for different slip frequencies $f_s = \omega/2\pi$, where typical rotor parameters as listed in Tab. I have been used. It can be observed that the current density is significantly increased close to the surface of the sphere for higher values of f_s due to the skin effect. The overall rotor losses have been calculated by integrating (12) over the entire volume of the rotor as (cf. [5])

$$P_{\mathrm{EC}} = \int_0^{2\pi}\int_0^{\pi}\int_0^{a} p_{\mathrm{EC}}\ r^2\sin(\theta)\mathrm{d}r\mathrm{d}\theta\mathrm{d}\varphi. \tag{13}$$

The results are displayed for the considered cases of f_s in the legend of Fig 4. These losses are significantly increased for high slip frequencies.

Figure 5 shows a plot of the corresponding torque as obtained from (9) normalized to its maximum value $T_{\max}$ as well as the rotor losses P_{EC} for varying slip frequency.

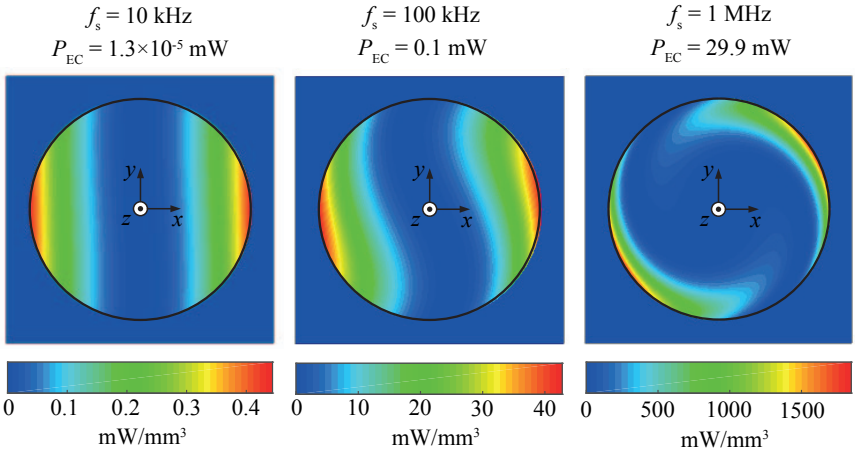

Fig. 4: Loss density distribution inside the spherical rotor in the xy-plane for different slip frequencies at the instant where $\vec{B}$ is pointing into the positive x direction (as displayed in Fig. 3).

TABLE I: Rotor Parameters

Material	100Cr6
μ_r	4
σ	4.5 MS/m
a	0.5 mm
κ	47 W/(m·K)

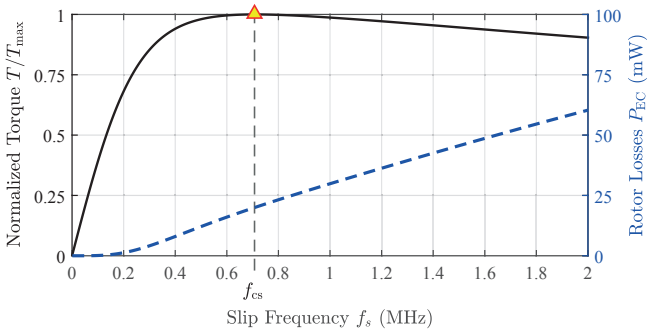

Fig. 5: Achievable torque and rotor losses dependent on the slip frequency ($a = 0.5$ mm).

It can be observed that the torque characteristics exhibits a clear maximum at the critical slip frequency f_{cs}, while the rotor losses increase almost linearly with the slip frequency.

A. Thermal Model of the Rotor

A thermal model of the rotor is required to predict its heating due to eddy current losses as discussed in the previous section. Due to the small dimensions of the rotor and the high thermal conductivity κ of the used material (cf. Tab. I), it is assumed that the losses cause a homogeneous heating of the rotor, despite the uneven loss density distribution. As the rotor is contactlessly levitated and accelerated inside a vacuum, it is also assumed that no heat is transferred to the ambient by means of conduction or convection ($P_{\mathrm{conv}} = 0$). Instead,

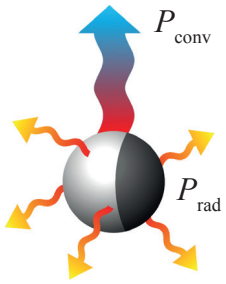

Fig. 6: Heat transfer mechanisms of a rotor with black marking.

power is only transferred to the ambient by radiation, which is described by the relation [6]

$$P_{\mathrm{rad}} = \epsilon \cdot \sigma_B \cdot A_{\mathrm{r}} \cdot \left(\theta_{\mathrm{r}}^4 - \theta_{\mathrm{amb}}^4\right), \tag{14}$$

where ϵ, σ_{B}, $A_{\mathrm{r}} = 4\pi a^2$, θ_{r}, and θ_{amb}, denote the emissivity, the Stefan-Boltzmann constant, the surface area of the rotor, the absolute temperature of the rotor, and the absolute ambient temperature, respectively. An ambient temperature of $\theta_{\mathrm{amb}} = 298$ K (25°C) has been used in the further calculations. The emissivity, which is dependent on the surface properties, is approximately $\epsilon_1 = 0.075$ for a polished stainless steel rotor. For measuring the rotational speed of the rotor, half of its surface area is covered by a black marking, as shown in Fig. 6, which has a significantly higher emissivity factor of $\epsilon_2 =\sim 0.9$. This results in

$$P_{\mathrm{rad}} = [\epsilon_1 + \epsilon_2] \cdot 2\pi a^2 \sigma_B \cdot \left(\theta_{\mathrm{r}}^4 - \theta_{\mathrm{amb}}^4\right). \tag{15}$$

The resulting rotor temperature can be obtained by setting $P_{\mathrm{EC}} = P_{\mathrm{rad}}$ and solving (14), (15) for θ_{r} numerically. This calculation of the rotor temperature is based on the assumption that the eddy current losses are the only occurring rotor losses. All other losses, such as air friction losses and hysteresis losses have been neglected. This is valid in first approximation, as the experiments are carried out in vacuum

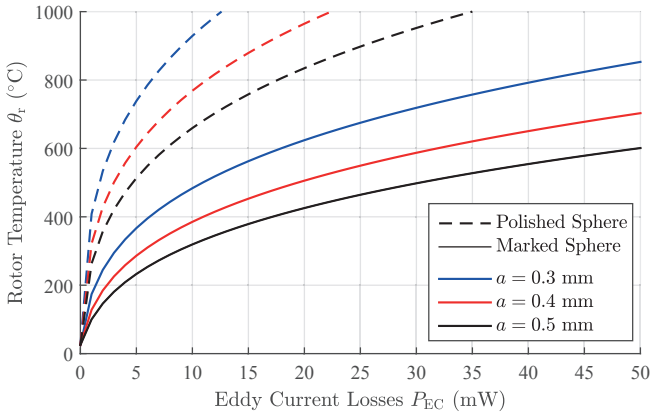

Fig. 7: Rotor temperature dependent on dissipated rotor losses for polished and marked spheres of different radii.

and hysteresis losses become insignificant at high rotational speeds [7]. Figure 7 shows the expected temperature for different rotor radii a (material parameters as listed in Tab. I) with and without the black marking dependent on the rotor loss power P_{EC}. It can be observed that the marking of the rotor results in a significant decrease of its temperature, due to the much higher emissivity of black color. Moreover, it is apparent that the rotor reaches high temperatures even for low loss powers, due to the absence of convection and conduction.

The presented model allows to assess the rotor temperature in steady state throughout the acceleration process, including the instance shortly before it explodes due to the exceedance of the ultimate tensile strength of the material.

V. Thermal Optimization

Based on the knowledge of the torque characteristics and the thermal behavior of the rotor, it is possible to choose the slip frequency such that a high torque per temperature increase of the rotor is generated. For that purpose, the torque-temperature ratio

$$TTR = \frac{T}{\theta_{\mathrm{r}}}, \tag{16}$$

has been calculated for varying slip frequency and different rotor radii assuming a marked rotor. The results are displayed in Fig. 8 for an external flux density magnitude of $B_0 = 5$ mT, which shows that a distinct maximum for this ratio can be obtained at the slip frequency f_{TTR}. This frequency is significantly lower than the previously obtained critical slip frequency f_{cs}, due to the highly nonlinear behavior of the rotor temperature. Moreover, it is also dependent on the magnitude of the external flux density and is decreased as B_0 is increased. This dependency is illustrated in Fig. 9 for a rotor with radius $a = 0.5$ mm. Fig. 9 also shows the value of TTR for operation of the motor with a slip frequency equal to f_{TTR} (maximum attainable value of TTR).

The slip frequency f_{TTR}, which yields the optimal ratio between T and θ_{r}, has been used to calculate absolute values for the rotor torque and temperature for various values of

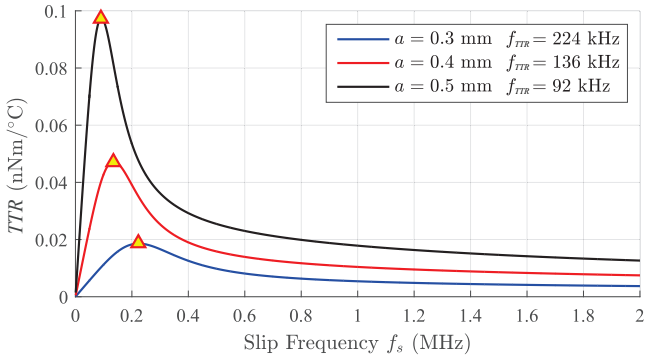

Fig. 8: Ratio of rotor torque and temperature for varying slip frequency and different rotor radii ($B_0 = 5$ mT).

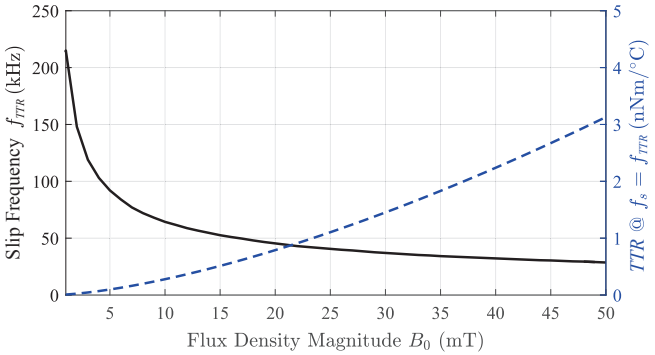

Fig. 9: Optimal slip frequency f_{TTR} and torque-temperature ratio as a function of the external flux density magnitude B_0 ($a = 0.5$ mm).

the flux density magnitude B_0. The results are shown in Fig. 10. It is demonstrated that even for the higher values of the motor torque, rotor temperatures far below the melting temperature of the rotor material can be maintained by choosing $f_s = f_{TTR}$. For these operating conditions, the additional torque originates from an increase of the external flux density only, while the current density inside the rotor is kept relatively constant. As a result, the overall rotor losses are kept at an equal level, yielding a rotor temperature of about 34°C. With this figure, it is easily possible to determine the resulting torque and therefore the duration of an acceleration experiment to a desired rotational speed for a given flux density magnitude.

As illustrated above, practical operating conditions at which the melting temperature of the rotor is exceeded can easily be attained. If the motor is operated with a slip frequency other than f_{TTR}, excessive values of the rotor temperature can be reached albeit the torque being relatively low. Even if this is not the case, temperatures may be obtained at which the tensile strength of the rotor material is significantly lowered, causing failure at lower rotational speeds than otherwise possible. Consequently, choosing the correct slip frequency as demonstrated in this work is crucial in order to achieve ultra-high rotational speeds that are not

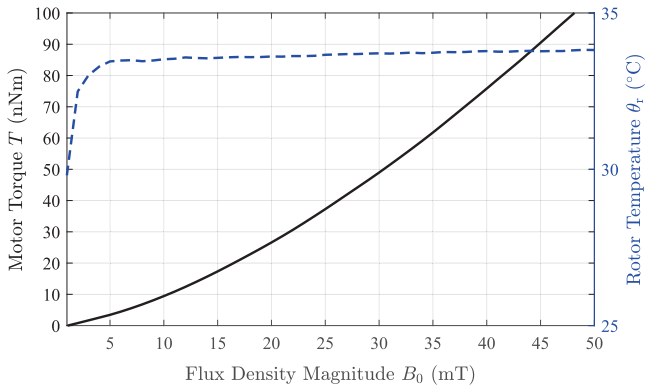

Fig. 10: Motor torque and rotor temperature at $f_s = f_{TTR}$ for varying external flux density magnitude B_0 ($a = 0.5$ mm).

impaired by a weakening of the rotor material.

VI. Conclusion

An analytical thermal model for the spherical rotor of an ultra-high speed spinning ball motor, which is capable of achieving rotational speeds beyond 25 Mrpm, has been presented. This model allows to determine the resulting rotor temperature for a given set of operating conditions of the motor. Inversely, it provides a guideline for choosing the operating conditions of the motor for maintaining a defined upper level of the rotor temperature.

The presented findings allow the assessment of the influence of the drive system on the mechanical properties of the rotor and, therefore, its behavior under high centrifugal loading, such as occurring at ultra-high rotational speeds.

References

[1] C. Zwyssig, J. Kolar, and S. Round, "Megaspeed drive systems: Pushing beyond 1 million r/min," *IEEE/ASME Trans. Mechatronics*, vol. 14, no. 5, pp. 564–574, 2009. [Online]. Available: http://ieeexplore.ieee.org/stamp/stamp.jsp?arnumber=481320

[2] J. W. Beams, J. L. Young, and J. W. Moore, "The production of high centrifugal fields," *Journal of Applied Physics*, vol. 17, no. 11, pp. 886–890, 1946. [Online]. Available: http://scitation.aip.org/content/aip/journal/jap/17/11/10.1063/1.1707658

[3] G. Löwisch and M. Dalgic, "The influence of the temperature on the stress-strain curves of a bearing steel and a case hardening steel," *Materialwissenschaft und Werkstofftechnik*, vol. 37, no. 1, pp. 134–141, 2006.

[4] H. Bhadeshia, "Steels for bearings," *Progress in materials Science*, vol. 57, no. 2, pp. 268–435, 2012.

[5] T. Reichert, T. Nussbaumer, and J. W. Kolar, "Complete analytical solution of electromagnetic field problem of high-speed spinning ball," *Journal of Applied Physics*, vol. 112, no. 10, pp. –, 2012. [Online]. Available: http://scitation.aip.org/content/aip/journal/jap/112/10/10.1063/1.4765676

[6] M. J. Moran, H. N. Shapiro, D. D. Boettner, and M. B. Bailey, *Fundamentals of engineering thermodynamics*. John Wiley & Sons, 2010.

[7] K. Yamazaki, A. Suzuki, M. Ohto, and T. Takakura, "Harmonic loss and torque analysis of high-speed induction motors," *Industry Applications, IEEE Transactions on*, vol. 48, no. 3, pp. 933–941, 2012.

VII. Biographies

Marcel Schuck (S'13) received the B.Sc. degree in Electrical and Computer Engineering from the Technische Universität Darmstadt, Germany, in 2011 and the M.Sc. degree in the same field from the University of Illinois at Urbana-Champaign, in 2013. He received an MBA degree from the Collège des Ingénieurs, Paris, France, in 2014. He is currently working toward the Ph.D. degree at the Swiss Federal Institute of Technology (ETH) Zurich, Switzerland. His research focus is on ultra-high speed bearingless machines.

Daniel Steinert (S'13) was born in Roth, Germany, in 1987. He received the M.Sc. degree in mechatronics from Dresden University of Technology, Dresden, Germany, in 2012, where he focused on micromechatronics and precision engineering. Since 2012, he has been working toward the Ph.D. degree at the Power Electronic Systems Laboratory, Swiss Federal Institute of Technology Zurich (ETH Zurich), Zurich, Switzerland, where he works on high-speed bearingless motors. His current research is focused on bearingless motor topologies, control concepts, losses, and applications of bearingless motors.

Johann W. Kolar (S'89-M'91-SM'04-F'10) received the M.Sc. and Ph.D. degrees (summa cum laude) from Vienna University of Technology, Vienna, Austria. He is currently a Full Professor with and the Head of the Power Electronic Systems Laboratory, Swiss Federal Institute of Technology Zurich (ETH Zurich), Zurich, Switzerland. He has proposed numerous novel pulsewidth-modulation converter topologies and modulation and control concepts, published more than 650 scientific papers in international journals and conference proceedings, and filed more than 110 patents. The focus of his current research is on ultracompact and ultraefficient converter topologies employing latest power semiconductor technology (SiC and GaN), wireless power transfer, solid-state transformers, power supplies on chip, and ultra-high speed and bearingless motors. Prof. Kolar was a recipient of 21 IEEE TRANSACTIONS and conference prize paper awards, the 2014 SEMIKRON Innovation Award, the 2014 IEEE Power Electronics Society R. David Middlebrook Award, and the ETH Zurich Golden Owl Award for Excellence in Teaching.